REPORT DOCUMENTATION PAGE

Form Approved
OMB No. 0704-0188

1. REPORT DATE *(DD-MM-YYYY)*	2. REPORT TYPE	3. DATES COVERED *(From - To)*
28-01-2011	FInal	05-04-2006 - 31-12-2010

4. TITLE AND SUBTITLE
Use of the Polarized Radiance Distribution Camera System in the RADYO program

5a. CONTRACT NUMBER

5b. GRANT NUMBER
N00014-06-1-0720

5c. PROGRAM ELEMENT NUMBER

6. AUTHOR(S)
Kenneth J Voss

5d. PROJECT NUMBER

5e. TASK NUMBER

5f. WORK UNIT NUMBER

7. PERFORMING ORGANIZATION NAME(S) AND ADDRESS(ES)
Physics Department, University of Miami
Coral Gables, FL. 33124

8. PERFORMING ORGANIZATION REPORT NUMBER

9. SPONSORING/MONITORING AGENCY NAME(S) AND ADDRESS(ES)
Office of Naval Research
875 North Randolph Street
Arlington VA. 22203-1995

10. SPONSOR/MONITOR'S ACRONYM(S)
ONR

11. SPONSORING/MONITORING AGENCY REPORT NUMBER

12. DISTRIBUTION AVAILABILITY STATEMENT
Approved for Public Release;distribution is unlimited

13. SUPPLEMENTARY NOTES

14. ABSTRACT
The spectral polarized radiance distribution provides the most complete description of the light field that can be measured. However, this is a very difficult parameter to measure near the surface because of its large dynamic range, changes in the sky, and waves at the air-sea interface. To measure the Stokes vector of the light field, which describes the polarization of the light field, requires the combination of four images, all of which must be obtained simultaneously. To achieve this, we recently developed the Downwelling Polarized Radiance Distribution Camera System (DPOL) under support from the ONR DURIP program. The work covered under this grant supported using this new instrument, developing a polarized sky camera, and making sunphotometer measurements during the RaDYO field programs experiments in San Diego (Scripps Pier), Santa Barbara Channel, and off of Hawaii.

15. SUBJECT TERMS
Polarization, Radiance Distribution

16. SECURITY CLASSIFICATION OF:			17. LIMITATION OF ABSTRACT	18. NUMBER OF PAGES	19a. NAME OF RESPONSIBLE PERSON
a. REPORT	b. ABSTRACT	c. THIS PAGE		24	Kenneth J Voss
					19b. TELEPONE NUMBER *(Include area code)* 305 284 2323 ext 2

INSTRUCTIONS FOR COMPLETING SF 298

1. REPORT DATE. Full publication date, including day, month, if available. Must cite at lest the year and be Year 2000 compliant, e.g., 30-06-1998; xx-08-1998; xx-xx-1998.

2. REPORT TYPE. State the type of report, such as final, technical, interim, memorandum, master's thesis, progress, quarterly, research, special, group study, etc.

3. DATES COVERED. Indicate the time during which the work was performed and the report was written, e.g., Jun 1997 - Jun 1998; 1-10 Jun 1996; May - Nov 1998; Nov 1998.

4. TITLE. Enter title and subtitle with volume number and part number, if applicable. On classified documents, enter the title classification in parentheses.

5a. CONTRACT NUMBER. Enter all contract numbers as they appear in the report, e.g. F33615-86-C-5169.

5b. GRANT NUMBER. Enter all grant numbers as they appear in the report, e.g. 1F665702D1257.

5c. PROGRAM ELEMENT NUMBER. Enter all program element numbers as they appear in the report, e.g. AFOSR-82-1234.

5d. PROJECT NUMBER. Enter al project numbers as they appear in the report, e.g. 1F665702D1257; ILIR.

5e. TASK NUMBER. Enter all task numbers as they appear in the report, e.g. 05; RF0330201; T4112.

5f. WORK UNIT NUMBER. Enter all work unit numbers as they appear in the report, e.g. 001; AFAPL30480105.

6. AUTHOR(S). Enter name(s) of person(s) responsible for writing the report, performing the research, or credited with the content of the report. The form of entry is the last name, first name, middle initial, and additional qualifiers separated by commas, e.g. Smith, Richard, Jr.

7. PERFORMING ORGANIZATION NAME(S) AND ADDRESS(ES). Self-explanatory.

8. PERFORMING ORGANIZATION REPORT NUMBER. Enter all unique alphanumeric report numbers assigned by the performing organization, e.g. BRL-1234; AFWL-TR-85-4017-Vol-21-PT-2.

9. SPONSORING/MONITORS AGENCY NAME(S) AND ADDRESS(ES). Enter the name and address of the organization(s) financially responsible for and monitoring the work.

10. SPONSOR/MONITOR'S ACRONYM(S). Enter, if available, e.g. BRL, ARDEC, NADC.

11. SPONSOR/MONITOR'S REPORT NUMBER(S). Enter report number as assigned by the sponsoring/ monitoring agency, if available, e.g. BRL-TR-829; -215.

12. DISTRIBUTION/AVAILABILITY STATEMENT. Use agency-mandated availability statements to indicate the public availability or distribution limitations of the report. If additional limitations/restrictions or special markings are indicated, follow agency authorization procedures, e.g. RD/FRD, PROPIN, ITAR, etc. Include copyright information.

13. SUPPLEMENTARY NOTES. Enter information not included elsewhere such as: prepared in cooperation with; translation of; report supersedes; old edition number, etc.

14. ABSTRACT. A brief (approximately 200 words) factual summary of the most significant information.

15. SUBJECT TERMS. Key words or phrases identifying major concepts in the report.

16. SECURITY CLASSIFICATION. Enter security classification in accordance with security classification regulations, e.g. U, C, S, etc. If this form contains classified information, stamp classification level on the top and bottom of this page.

17. LIMITATION OF ABSTRACT. This block must be completed to assign a distribution limitation to the abstract. Enter UU (Unclassified Unlimited) or SAR (Same as Report). An entry in this block is necessary if the abstract is to be limited.

Final Report:
Use of the Polarized Radiance Distribution Camera system in the RADYO program

Kenneth J. Voss
Physics Department, University of Miami
Coral Gables, Fl. 33124
phone: (305) 284-2323 ext 2 fax: (305) 284-4222 email: voss@physics.miami.edu

Award Number: N000140610720
http://optics.physics.miami.edu

INTRODUCTION:

The spectral polarized radiance distribution provides the most complete description of the light field that can be measured. However, this is a very difficult parameter to measure near the surface because of its large dynamic range, changes in the sky, and waves at the air-sea interface. To measure the Stokes vector of the light field, which describes the polarization of the light field, requires the combination of four images, all of which must be obtained simultaneously. To achieve this, we recently developed the Downwelling Polarized Radiance Distribution Camera System (DPOL) under support from the ONR DURIP program. The work covered under this grant supported using this new instrument, developing a polarized sky camera, and making sunphotometer measurements during the RaDYO field programs experiments in San Diego (Scripps Pier), Santa Barbara Channel, and off of Hawaii.

The DPOL instrument follows in the footsteps of other radiance distribution instruments we have built (Voss and Liu, 1997;Voss and Chapin, 2005). This instrument consists of 4 fisheye camera lenses with polarizer's behind each lens in a different orientation. Behind each polarizer is a coherent fiber bundle and these 4 bundles are brought together and imaged onto a CCD camera (Apogee Alta E2000) through a filter changer consisting of 7 spectral filters ranging from 410 nm to 650 nm. Thus, in a single image we obtain 4 separate fisheye images (whole hemisphere) of the same scene, each with different polarization information. These 4 images allow us to calculate the Stokes parameters in a hemisphere of directions. An orientation sensor in the system provides us information on the roll, pitch and yaw of the instrument at the time the image is captured and the pressure sensor data can be used to find the depth. The integration time for each image in the seawater varies from 3 ms to 1 s depending upon the spectral filter used, the brightness of the sky, and the instrument depth. This instrument can be used for the measurement of the upwelling radiance distribution in the ocean as well, but this ONR work, because of the RaDYO objectives, focused on the downwelling light field.

As background, to describe the polarized radiance distribution, the most convenient representation is the Stokes vector, derived by Stokes in 1852. The electric field vector **E** of the light field propagating in the **z** direction can be decomposed into two components,

E_l and E_r, which represent the magnitude and phase of the electric field vectors parallel (**l**) and perpendicular (**r**) to a reference plane:

$$\mathbf{E} = E_l \mathbf{l} + E_r \mathbf{r} \qquad [1]$$

Such that **z** = **r** x **l** and the reference plane is the plane containing the direction of propagation and another convenient direction.

Considering a coherent electromagnetic wave propagating along the **z** direction with a frequency ω and the amplitudes and phases along **l** and **r** directions being a_l and δ_l respectively, then

$$\begin{aligned} E_l &= a_l \cos(kz - \omega t + \delta_l) \\ E_r &= a_r \cos(kz - \omega t + \delta_r) \end{aligned} \qquad [2]$$

Here k is the wave constant and λ the wavelength.

In general the tip of the electric vector described in [1] and [2] forms an ellipse and we can define the Stokes parameters in terms of the complex amplitudes of the wave as (Coulson, 1988; Van de Hulst, 1981)

$$\begin{aligned} I &= E_l E_l^* + E_r E_r^* = I_l + I_r \\ Q &= E_l E_l^* - E_r E_r^* = I_l - I_r = I \cos 2\beta \cos 2\chi \\ U &= E_l E_r^* + E_r E_l^* = I \cos 2\beta \sin 2\chi \\ V &= i(E_l E_r^* - E_r E_l^*) = I \sin 2\beta \end{aligned} \qquad [3]$$

Where we have assumed that the ellipse has a major axis (a) and a minor axis (b). The ellipticity is given by $\tan \beta = b/a$, which is 0 for linear polarization, -1 for left-handed and 1 for right-handed circular polarization. The orientation of the ellipse is given by the angle χ which is the angle made by the major axis with the direction **l**.

From [3], it can be easily shown that

$$I^2 \geq Q^2 + U^2 + V^2 \qquad [4]$$

and the degree of polarization (P), the plane of polarization and the ellipticity are, respectively, given by,

$$P = (Q^2 + U^2 + V^2)^{1/2} / I$$

$$\tan 2\chi = U / Q$$

$$\sin 2\beta = \frac{V}{(Q^2 + U^2 + V^2)^{1/2}}$$

[5]

One should transform the Stokes parameter measured in the laboratory frame into a more common frame such as the sky frame (Liu, 1996). In the sky frame (Fig. 1), we consider the light propagating along **z = r x l** direction and χ is the plane of polarization measured from **l** to **r**. Then,

$$Q = I_l - I_r$$
$$U = I_{+45} - I_{-45} \qquad [6]$$

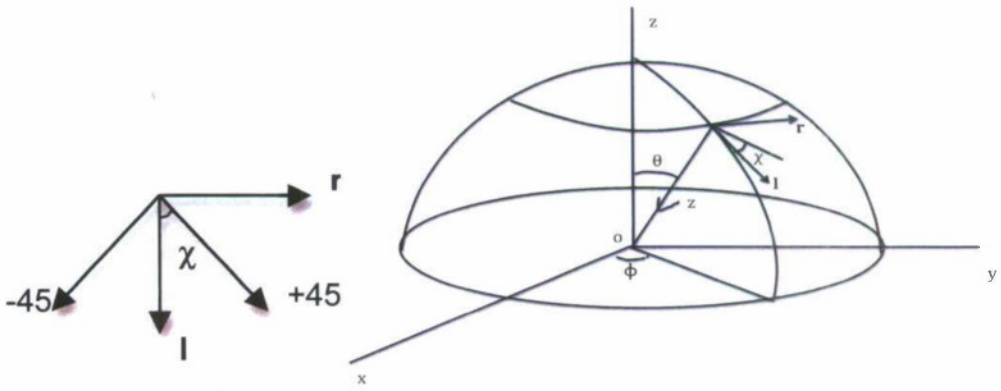

Figure 1. Illustration of the coordinate system in the sky frame.

For the transformation of the Stokes parameters from lab frame (x,y) to sky frame (x′,y′) we consider the rotation of the (x,y) axes by an angle γ. By definition, the intensity I is invariant under such rotation and as is seen from Eq. [3], the V is also invariant as it is independent of χ and only depends on intensity and β. Then the Stokes parameters in the new frame are given by (Coulson, 1988),

$$I' = I$$
$$Q' = Q\cos 2\gamma + U\sin 2\gamma$$
$$U' = -Q\sin 2\gamma + U\cos 2\gamma \qquad [7]$$
$$V' = V$$

INSTRUMENT DESCRIPTION

As stated before, this new system is based around a fisheye lens system, to enable a whole hemisphere of information to be found. The system will be described in more detail now, following the path of light entering the system.

The first element the light enters is a glass hemispherical dome window. These are custom windows, provided through Outland Technology, and have a 3.00" interior diameter and 3.25" exterior diameter. Presently there are no coatings on these windows.

After the window, light is collected with a fisheye lens. The fisheye lens used in these systems is the Coastal Optics c-mount fisheye lens, with a 2.16 mm focal length and is f/3.3. This lens focuses the light through the polarizer element onto the coherent fisheye

bundle. The polarization properties of the lenses were tested by looking at the extinction ratio resulting from fully polarized light entering the lens, and having either a crossed or parallel polarizer behind the lens. The extinction ratio was greater than 100:1 at all angles of incidence onto the system. The lens is mounted behind the dome in such a way as to make the effective first principal plane of the optical system at the center of curvature of the dome window. If this is done correctly, then the system will perform in water and in air equivalently.

Behind 3 of the fisheye lenses are linear polarizer's, while the other lens has a combination of a quarter wave plate and a linear polarizer. The 3 linear polarizer's are dichroic sheet polarizer's (Melles Griot, 03 FPG 019). Polarizer's are orientated at 0 deg, 60 deg, and 120 deg (angles relative to the first polarizer). The combination of the images with these polarizer orientations allows the linear polarization state of the light to be determined. The last fisheye has a combination of a broadband mica quarter wave plate (Melles Griot, 02 WRM001) and a polarizer to form a circular polarization analyzer. The combination of the 3 linear polarizer images allows the first three polarization stokes vectors to be calculated, while with the 4^{th} image all 4 Stokes parameters can be determined.

The image from each fisheye lens is focused onto the end of a custom coherent fiber bundle (Schott). Each leg of the fiber bundle is 4mm x 4mm, and made up of 10 um fibers. There is a custom fiber optic taper which adjusts the image size of the lens to the size of the optical fiber bundle. On the other end of the fiber, these 4 fiber bundles are brought together to form a 2 x 2 array of individual fisheye images. The grouped end of the fiber bundle is imaged onto the CCD camera using a lens relay system made up of 2 – 50mm lenses (Schott, 1G1650). In between the two relay lenses we place a filter changer (Optec IFW), which has 25.4 mm diameter interference filters to select the spectral band of interest.

We are using an Apogee, Alta E2000 camera in this system. This camera uses the Kodak KAI-4020 interline transfer array (1600 x 1200 pixels) and has an electronic shutter to allow very fast exposure times. In addition it has anti-blooming features to help stop bright features from washing out the rest of the image. This camera system has an Ethernet interface, so it is controlled from the surface with a laptop computer. Figure 2 shows a sample image with the system.

Also inside the camera housing is a gyro enhanced orientation sensor (3DM-GXI, Micro Strain), to give tilt, roll, and heading and a pressure transducer to give instrument depth. The instrument communicates to the surface over an Ethernet interface. We have also included an Ethernet to fiber converter, and use optical fiber to connect to the instrument to give us longer communication distances. There is an ethernet hub in the instrument that allows us to either use a fiber link, or a copper link, depending on the distance requirements.

Figure 2. Sample image from Polarization camera system. There are 4 separate fisheye images shown in this one camera image, the result of our quadfricated fiber bundle. Each small fisheye image carries different polarization information. Three of the images have linear polarizers in line with the image optical path. The remaining image contains a circular polarization analyzer. By combining these images, the 4 stokes vectors can be determined.

Figures 3 and 4 show pictures of the instrument as it has been developed.

DPOL CALIBRATIONS:

To obtain quantitative data from the system, we need to perform the following calibrations of the DPOL:

i. Spectral calibration
ii. Linearity characterization
iii. Flatfield calibration
iv. Angular (air and water) calibration
v. Rolloff calibration
vi. Polarization (linear and circular) calibration
vii. Absolute calibration
viii. Immersion calibration

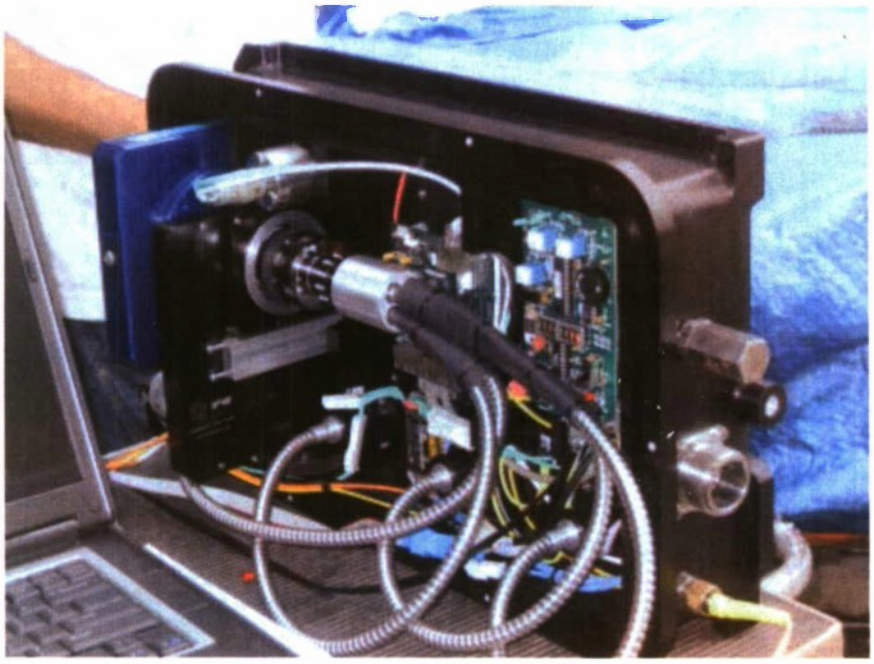

Figure 3. This is a picture of the interior of the polarization camera system. On the far left is the camera (the blue box), in front of which is the IFW filter chamber. The coherent fiber bundle is shown, with each leg going to fisheye lenses in the lower portion of the box. We also have a pressure transducer, tilt and roll indicator, and other associated electronics. The system is controlled by the laptop to the left of the picture.

Figure 4. Picture of the top of the polarization camera system. One can see the 4 fisheye lenses all aligned in a row. On the left are connectors to allow the system to be used, either over a dedicated cable (the big connector) or through the ROV system.

Steps i-ii, iv-v, and vii-viii are performed with the same technique as the non-polarized fisheye systems RADS and NuRADS (Voss and Zibordi 1989; Voss and Liu 1997; Voss and Chapin 2005). The Flatfield correction is particularly important with this system, and obviously the polarization calibration is required here.

Spectral Calibration: To measure the system relative spectral response, light from a monochromator (Optronics 740A) was introduced into the system, and an image collected. A small area in the middle of the illuminated portion of the array was sampled and averaged. The wavelength of the incoming light was varied 20 nm either side of the center band of the filter. From this we can calculate the center wavelength and full-width at half maximum (FWHM). The spectral bandpass of the system in each filter location are shown below in Fig. 5. The results of the spectral calibration are shown in Table 1. Note that the spectral filter wheel has positions for 8 filters, but one of these filter positions is taken up by a blank to provide a dark image during data collection.

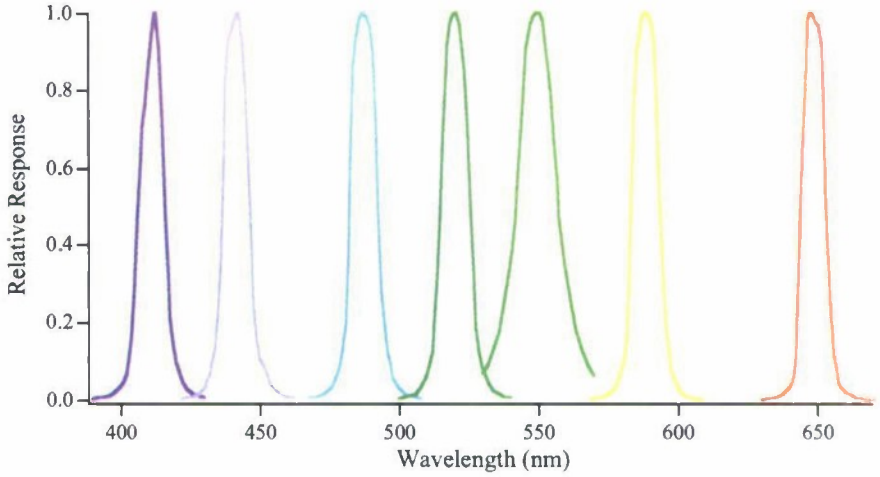

Figure 5) Relative spectral system response for the DPOL system.

Table 1) DPOL spectral calibration

Filter	Band Center (nm)	FWHM(full width at half maximum, nm)
1	411.1	9.7
2	441.6	9.9
3	487.7	10.4
4	520.6	10.8
5	550.1	15.3
6	589.1	10.3
7	649.2	9.2

Linearity Calibration: In this calibration we place the camera at a particular distance from a uniform source of light and take images with different exposure times, each time taking the corresponding dark counts. Then we plot a graph of camera counts versus the exposure time (or the shutter speed). We found that the counts are linear down to 7 ms exposure time (Fig. 6).

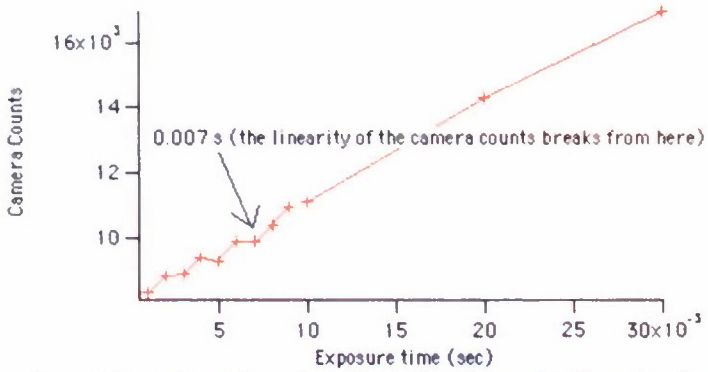

Figure 6. Linearity calibration showing that the linearity breaks from 0.007s exposure time.

Flatfield: Because of the optical fiber bundle, the field of view of even a uniform source does not produce a uniform image. The fiber bundle image has lines running through it due to absorbing layers that are put into the bundle to reduce fiber cross talk. In addition some fibers transmit better than others. Therefore, we need to perform a calibration to improve the image qualitatively and quantitatively. To do this calibration we expose the ends of the individual fiber bundles to a uniform source, through the spectral filter and lens relay system, and on to the camera. In this process we take approximately 20 to 30 images for each spectral filter, pointing the ends of each bundle towards a 1 meter integration sphere. These images are then averaged together to form the flatfield image that is used in the rest of the calibration, and in data reduction. Figure 7 is an example image resulting from the fibers being directly illuminated by the light from an integration sphere. Fig. 8 shows the effect of the flatfield correction on a horizontal line of data. The high spatial frequency noise in the original data is caused by the coherent fiber bundle, while the larger, lower spatial frequency problems originate in the joining of the fiber bundle and a fiber optic taper.

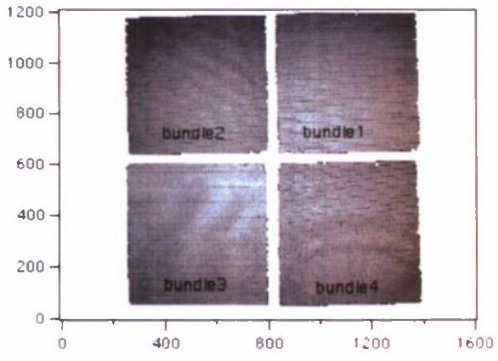

Figure 7. The image resulting from illuminating the ends of the fibers with an integrating sphere.

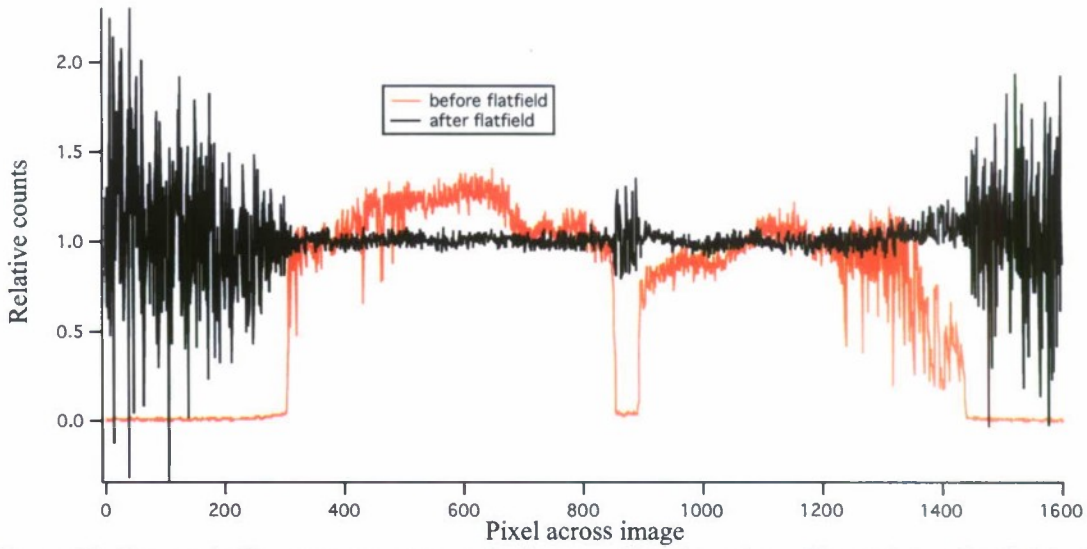

Figure 8) Example line across a sample image showing the effect of the flatfield. The edges of the flatfield, where the large oscillations happen, are out of the data region, and are cut off in later processing.

Angular calibration: The system must also undergo an angular calibration. This is simply done by placing a bright, almost point source several meters from the camera. The camera system is rotated, and the position of the point source in the image is recorded. This is then used to find the factor that relates the radius on the image plane to angular space. This must be done for each lens, as they will be slightly different. It also must be done in water, to account for any effects of the dome window. Table 2 shows these factors for the four lenses in the last calibration. One of the important steps in the instrument construction is to place the effective 1st principal plane of the optics in the center of curvature of the dome window. A test for how well this is done is to compare the conversion factors for this calibration step between the air measurements and in-water measurements. As can be seen below, these factors are within 1.3% of each other, and for the most part within the estimated error of the factor.

Table 2) Lens radius-to-degree conversion factors

Lens	in water	in air
1	0.343± 0.006	0.347± 0.004
2	0.342± 0.005	0.339± 0.002
3	0.350± 0.005	0.347± 0.002
4	0.349± 0.003	0.345± 0.001

Rolloff: The next requirement is to account for lens rolloff effects in the fisheye system. In this case the system is tested as a whole and the fisheye lens is pointed into the integrating sphere port. Images are obtained with the system looking into the port at many angles, to map out the response of each lens. Figure 9 shows the Rolloff factor for each lens. As can be seen, this is a significant affect near the edge of the image. For

reference, a pixel radius of 250 corresponds to a zenith angle of approximately 80 degrees.

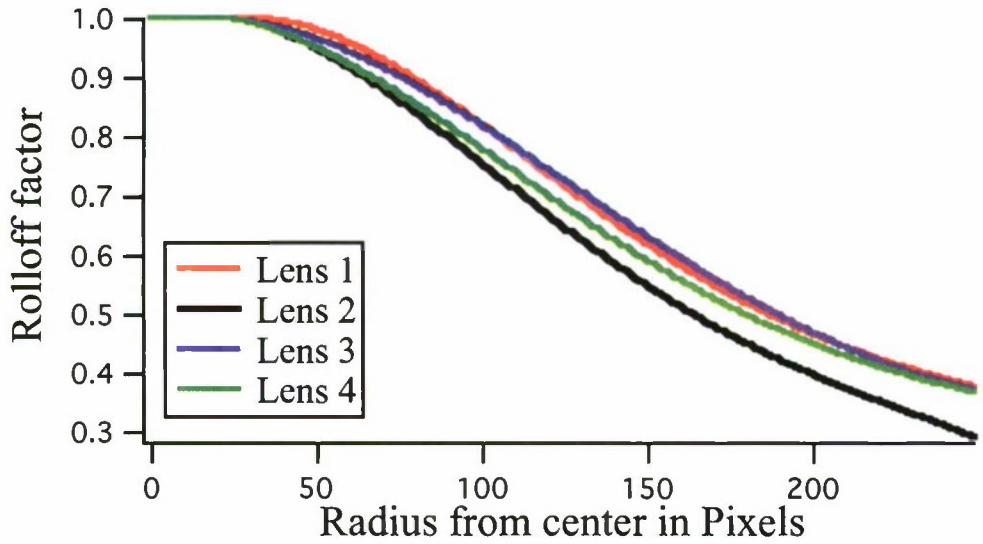

Figure 9) Rolloff factor as a function of radius from center of image, for each lens.

Polarization calibration: To get polarization information from the images, we must understand how to combine the 3 or 4 images to get the polarization stokes vector. Various papers have been published on how to accomplish this (for example Tyo, 1998). As with most calibration steps, the basic premise is to introduce light with known characteristics (in this case polarization), then see how the instrument responds. For our calibration, we placed a polarizer between the lens to be measured and an integrating sphere that provided a uniform source of unpolarized radiance. The polarizer was rotated through 180 degrees and an image was obtained at each 10 degrees of this polarizer angle. Because of the physical layout of the instrument, and the port size of the integrating sphere, we had to do this sequentially for each lens. It was also necessary to do this for each spectral filter. For each image, an area (5 x 5 pixels) in the center of the illuminated part of the array is extracted as representing the response of the system to that polarization state.

Many authors have chosen to use a polarization calibration such as this to determine the effective system Mueller matrix for each polarizer position or, in our case, lens. Once this Mueller matrix is determined, the matrix can be inverted, and this inverted matrix is used to determine the unknown stokes vector of incoming light in the experimental setting. In our case we take the 3 or 4 lens readings for the same polarizer position, and compare this with what we expect the stokes vector to be (either I=1, Q = cos 2θ, or U = sin 2θ). We perform a multi-variable linear regression with the independent variables being the lens readings, and the dependent variable being I, Q, or U. In this way we can determine a 3 x 3 (in the case of the linear polarization information) transformation matrix. This transformation matrix can then be directly used to transform the input

intensity information from each lens into relative stokes vectors, and then after the absolute calibration into absolute Stokes vectors.

This calibration step was performed as described. To test the parameters determined, we can compare how well the expected Stokes vectors are retrieved. Figure 10 shows both the expected values for the Stokes vectors, as a function of polarizer angle, then the error in generating the stokes vectors with the transformation matrix. This error is represented by the difference (reconstruction – prediction) in the normalized stokes vector. The average error in these reconstructed vectors is significantly less than 0.02%, but the RMS difference is 0.014, 0.017, and 0.032 for I, Q, and U respectively. At this point we don't understand why U is not reproduced as well as the other elements. From Fig. 10 it appears as if the larger RMS for U is driven by a few angles in particular (0, 160, and 170 degrees). We have taken the 410 nm measurement out of this analysis, because the flux from the integrating sphere is too low to get an accurate inversion.

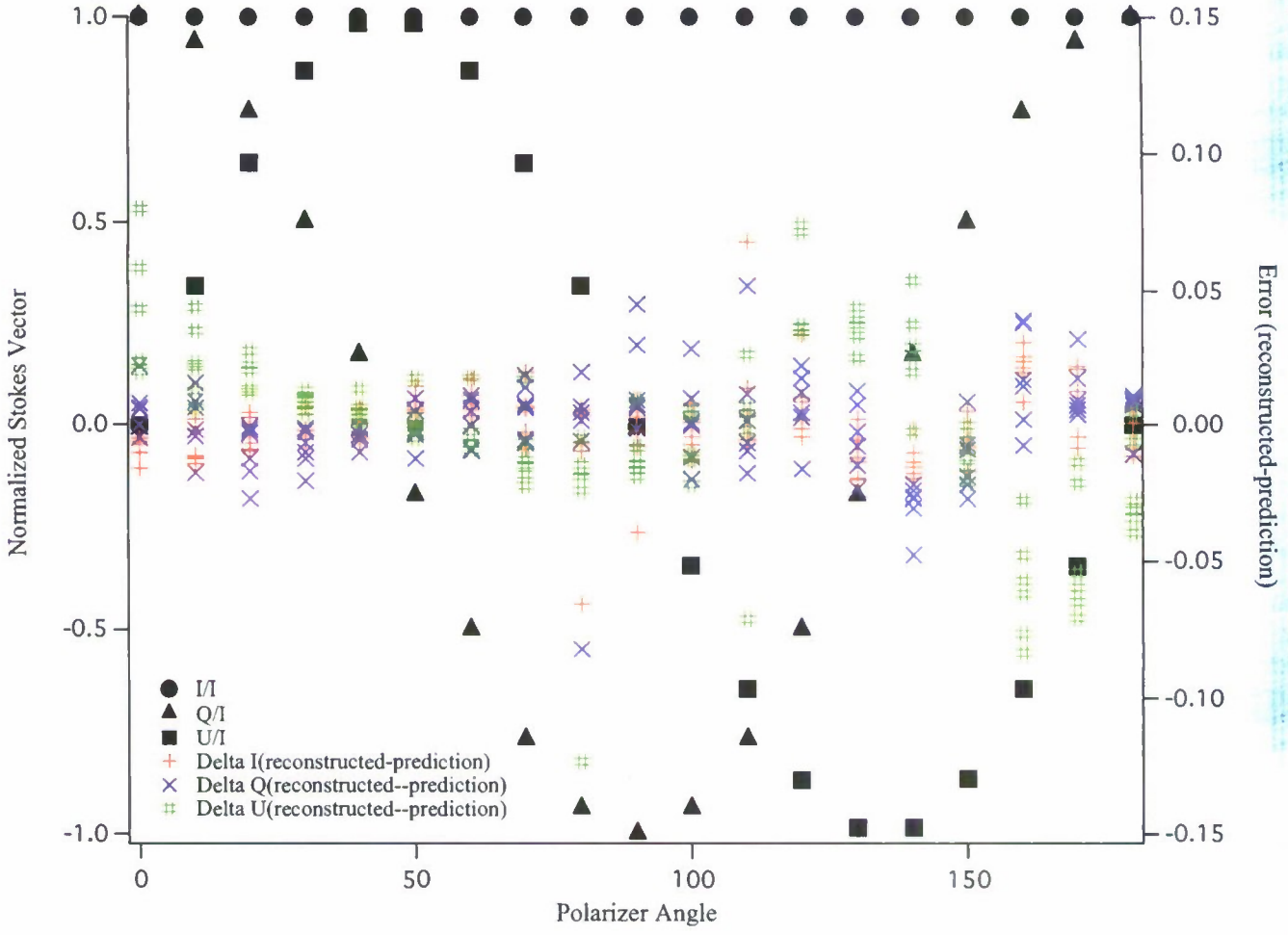

Figure 10) Normalized Stokes vectors and difference between reconstructed elements and prediction.

Absolute calibration: This step is done along the similarly to Voss and Zibordi (1989). However in this case the camera information must be run through the processing software to get the expected relative intensity, along with the other Stokes vectors. This intensity is adjusted with a calibration coefficient to obtain the absolute intensity in relative units. In the calibration procedure we take three separate images of the reflectance plaque. Because of the system size, we actually have to take the measurements for each lens at a slightly different time. We can then permutate through the images from each lens to get 27 estimates of the intensity (and Stokes vectors Q and U). When this was done, the standard deviation of these estimates was on the order of 0.5% or less, showing the values obtained are fairly uniform. In any case this calibration coefficient is included in the data reduction process.

Immersion calibration: An important calibration step for these systems is the immersion calibration. This step corrects for the difference between using the instrument in water as opposed to in air, where most of the calibration steps are performed. This is particularly important in this case, since the proper balancing of the values obtained from each lens is important for correctly calculating the stokes vectors, and this immersion coefficient can vary from lens to lens, depending on the individual dome and lens, because of the curvature of the dome.

The calibration has been described in Voss and Chapin (2005), for a scalar system, and is similar here. The system is placed in a barrel below an illuminated reflectance plaque. With the plaque stably illuminated, the water level above the camera is varied. A ratio is formed between the observed counts from an average of the image of the plaque when the dome window is dry versus barely covered with water. The values found for the immersion calibration are shown in Table 3. As can be seen there is a slight variation between the lenses, which is taken into account during data reduction.

Table 3) Lens Immersion coefficients, average over wavelength. Standard deviation is also shown.

Lens	Immersion coefficient	
1	1.812± 0.005	
2	1.811± 0.001	
3	1.793± 0.005	
4	1.798± 0.017 * (without one of 7 wavelengths it changes to	1.792± 0.006

DATA AND RESULTS:

We participated in three field experiments in the RaDyO program. Two of these were done off of the R/P Flip, one in Santa Barbara Channel (34 12.31' N and 119 37.725' W) on September 9-23, 2008 and in Hawaii (about 17 N and 155 W) on September 1-12, 2009. We will present data here from the Santa Barbara Channel experiment, during which GMT (Greenwich Mean Time) is 7 hours ahead of the local time. Most of the days we took the sky and in-water data together using two camera systems (DPOL and Sky-Cam.). The DPOL measurements are at various depths from near the surface to 70 meters.

In Figs. 11-22, we show the variation of the downwelling radiance distribution, the normalized Q and U vectors and the degree of polarization for the in-water (1 m to 30 m depth) and sky data from Santa Barbara Channel (SBC) experiment on September 22, 2008. We have selected data at one wavelength, 520nm. All images have been rotated to place the sun on the top of the figures. For DPOL (in-water) images, the white circle represents the boundary of the theoretical Snell's cone, determined by the critical angle. On the plots the zero on the horizontal scale is the zenith (the position of the instrument), the positive values are towards the sun and the negative values are away from the sun.

The underwater light field is linearly and partially polarized except for some elliptical polarization near the water surface and just beyond the critical angle (Ivanoff and Waterman, 1958). The surface waves are the main cause of the variation in the underwater light field near shallow depths (Synder and Dera, 1970) where (within few meters) the polarization behavior is influenced by the same factors as for the skylight within the Snell's cone (Waterman, 1954). The polarization outside the Snell's cone arises mainly from scattering and internal reflection at the water surface (Ivanoff, 1974). In the following images and plots one can see that near the surface the refracted sky light is the dominant source of radiance and polarization where the degree of (linear) polarization (DOP) in air and water are almost same. But, as one goes deeper in the water column, the effect of skylight decreases thereby decreasing the DOP in accordance with the earlier result by Ivanoff (Ivanoff, 1974). In water, the maximum DOP occurs in directions 60 to 90 degree to that of the solar beam (Waterman 1954, 1955; Ivanoff 1974). In air the maximum DOP occurs in a direction about 90 from the sun, which can be seen from the plots below.

Figures 11-13 are for the in-water data at 1 m depth and the corresponding sky data for 520 nm. The solar zenith angle (SZA) is 88 degree and the refracted solar zenith angle (SZA′) is 48 degree. The images were taken between 01:50 and 01:59 GMT on September 23, 2008. The sky is predominately clear, however there was a marine layer on the horizon and the sun is about to set. Wind speed is about 12 knots and there were small water waves and almost no white caps. Figures 11 (a and b) represent the radiance images for water (1m depth) and for sky. In the images the center represents the zenith, the edges represent the horizon (90 degree zenith) and the zenith angle is directly proportional to the radius from the center. The two cut-outs (arc's of missing data) seen around the edge of in-water images are portions of the images which are obstructed by the clamps which hold the glass dome windows on the instrument. We can see that the Snell's cone is well within the theoretical Snell's cone boundaries). In the radiance line plot for the principal plane (Figure 11.c), we see the two peaks for DPOL (black line) around the boundaries of the Snell's cone. The fluctuations in the plots are mainly caused by the water waves resulting in the instability of the DPOL near the surface.

In Figure 12, we can see that the minimum of the normalized Q lies opposite to the solar position along the principal plane. It is obvious, when comparing the sky and in-water pattern, that the in-water pattern is dominated, inside the Snell's circle, by the refracted sky light. Figures 13 (a) and (b) show the polarization patterns as seen in water (1 m

depth) and sky for 520 nm wavelength. The strongest polarization is within the Snell's cone.

The in-water data in Figs. 14-16 are at 5 m depth and the data were taken between 00:50 and 00:58 GMT on September 23, 2010. The solar zenith angle (SZA) is 77 degree and the refracted solar zenith angle (SZA′) is 47 degree. The sky and water surface conditions are similar to the previous case. The in water images are the average of 5 images. The radiance and the polarization behavior at this depth is almost the same as in the 1m case. However, we can see that there is more polarization outside the Snell's cone than in the 1 m case.

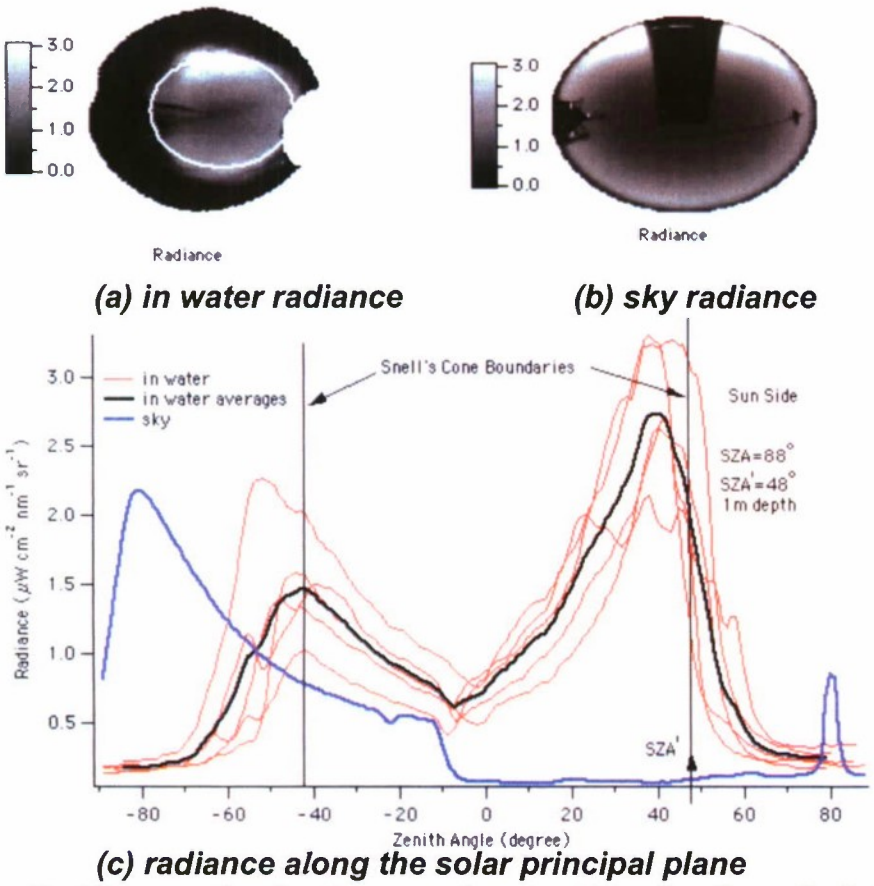

Figure 11. (a) Snell's cone is clearly seen almost within the theoretical Snell's boundary (white circle). On the left within the circle the two dark lines are images of the FLIP and the wire supporting the camera. The sun is at the top of the circle. (b) On the left we can see the top portion of the FLIP. The dark rectangular part on the top is the occulter used to block the sun. The horizontal line across the middle of the image is the line supporting the boom of the FLIP. (c) Downwelling radiance in the solar principal plane. Zero is zenith and positive is towards sun. We can see the two peaks around the edges of the Snell's cone, one towards sun and the other opposite to it.

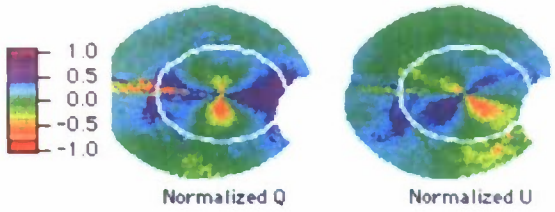

(a) in water

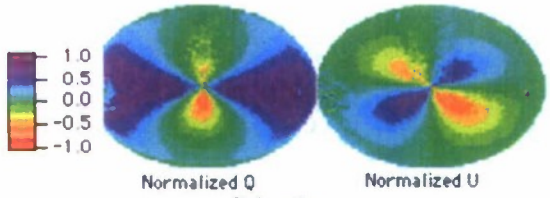

(b) sky

Figure 12. Normalized Q and U vectors in water (a) and in air (b). In both cases the minimum of normalized Q and U are at 45 degree to each other and the minimum Q lies opposite to the solar position along the solar principal axis.

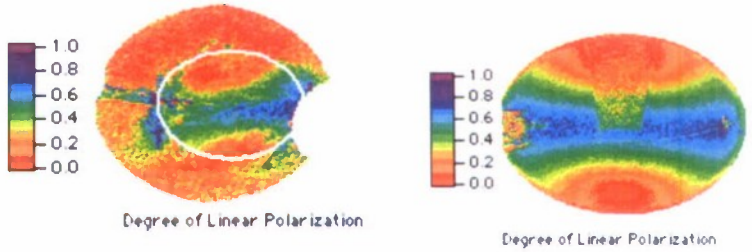

(a) in water (b) sky

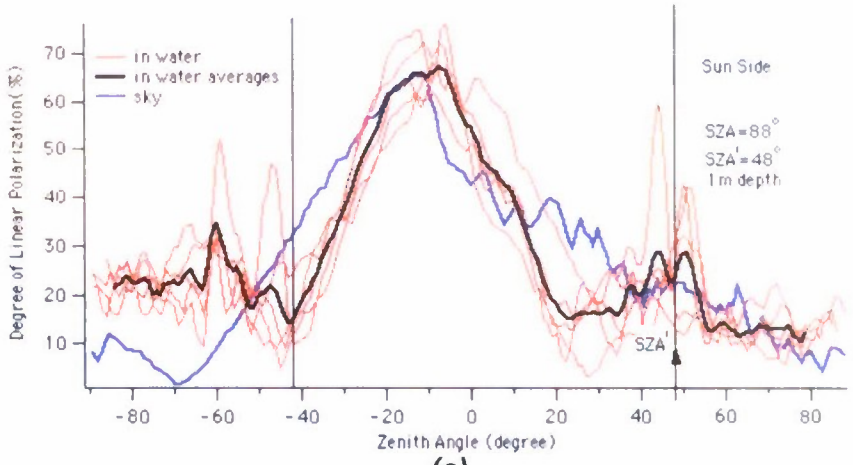

(c)

Figure 13.(a) and (b) in water (1 m depth) and sky polarization pattern for 520nm wavelength. (c) Variation of the degree of (linear) polarization with zenith angle along the solar principal plane. The sky and in water curves are similar in nature and both of them have almost the same DOP (about 65 %) which implies that the refracted sky light is the dominant source of polarization.

The in-water data for Figs. 17-19 are for 10 m depth and 520 nm. The in-water images are the average of 5 images. Solar zenith angle (SZA) is 58 degree and the refracted solar zenith angle (SZA′) is 40 degree. The images were taken between 23:15 and 23:23 GMT on September 22, 2008. The sky and water surface conditions are the same as in previous cases. In this case, there is no obvious break in the radiance at the edge of the Snell's cone. Also one can see the peak of the radiance is shifted towards the center from the refracted solar position, and that the polarization behavior outside the Snell's circle boundary is more noticeable than in the case of 5 m depth implying that scattering in the water is starting to have a significant affect in the data.

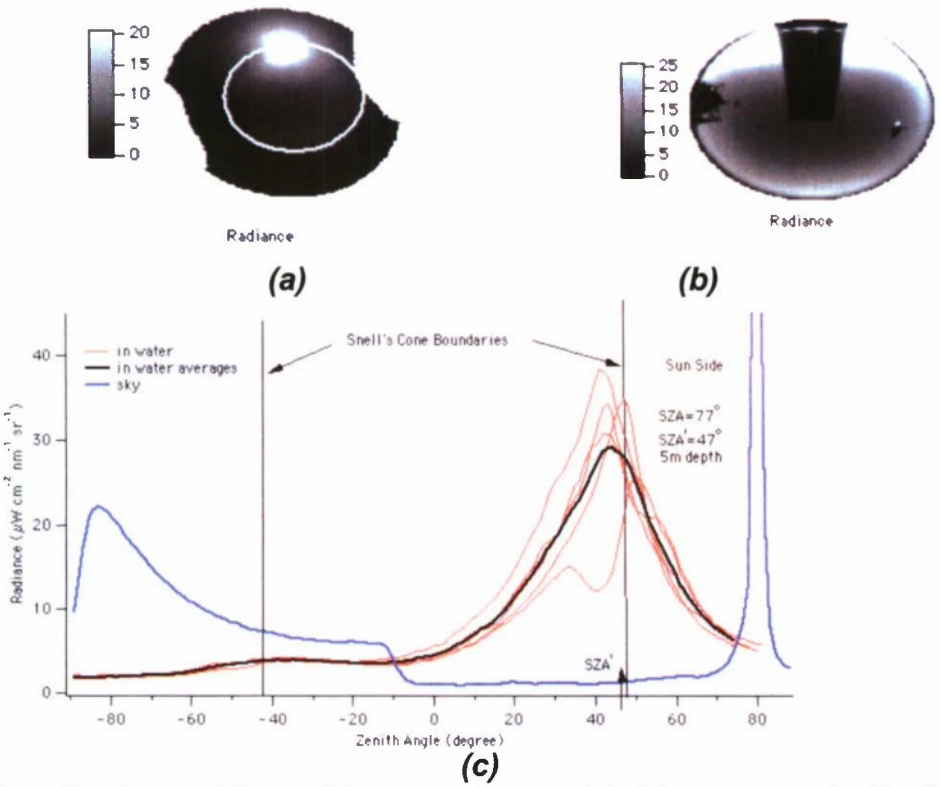

Figure 14. Similar to Figure 11, but at 5 m. This illustrates basically the same characteristics as in 1m depth. However, the maxim intensity toward the Snell's cone boundary on the opposite to sun is much less than on the sun side, and the boundary of the Snell's cone is not as distinct in the radiance.

The in-water data in Figs. 20-22 are for 30 m depth and both the sky and in-water data is at 520 nm wavelength. The in-water images are the average of 5 images. Solar zenith angle (SZA) is 34 degree and the refracted solar zenith angle (SZA′) is 25 degree. The time when the images were taken was between 19:45 and 19:53 GMT on September 22, 2008. The wind speed is about 5 Knots and the water is very calm. At this depth we can see that there is presence of polarization outside the Snell's cone, more than that of the previous cases. The maximum DOP in water is about 28%, which is about 27% less than that of the corresponding sky.

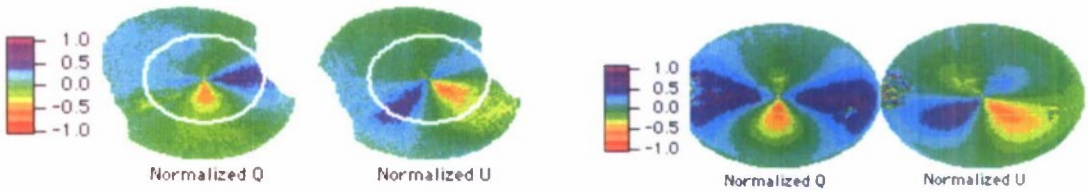

(a) *(b)*

Figure 15. Similar to Figure 12, but at 5 m. This is also similar to the result at 1 m, except that the polarization extends outside the Snell's cone more than that in 1m depth.

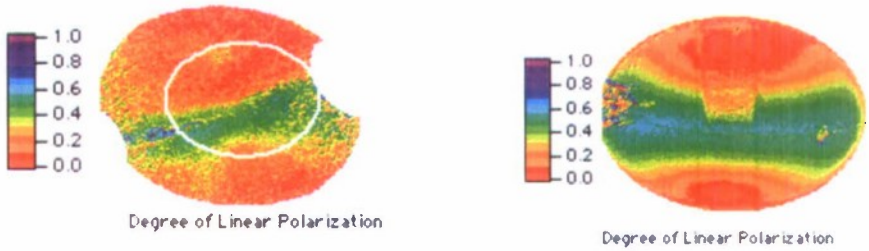

(a) *(b)*

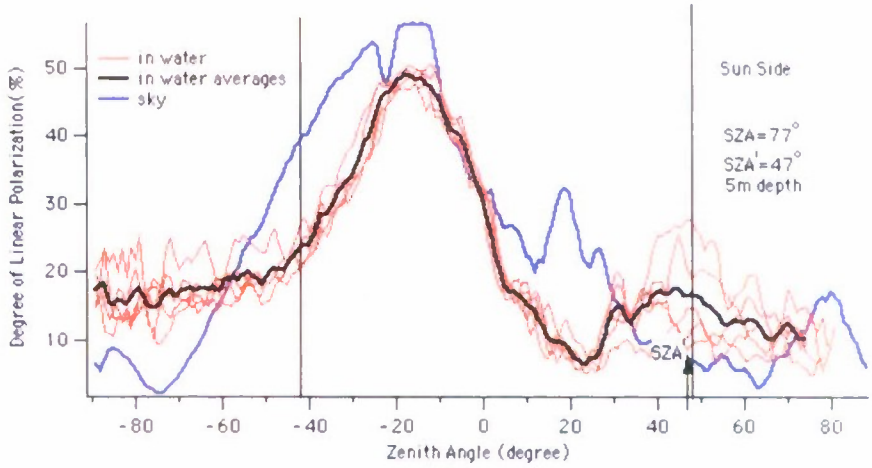

(c)

Figure 16. Similar to Figure 13, but at 5 m. The maximum DOP is about 45%.

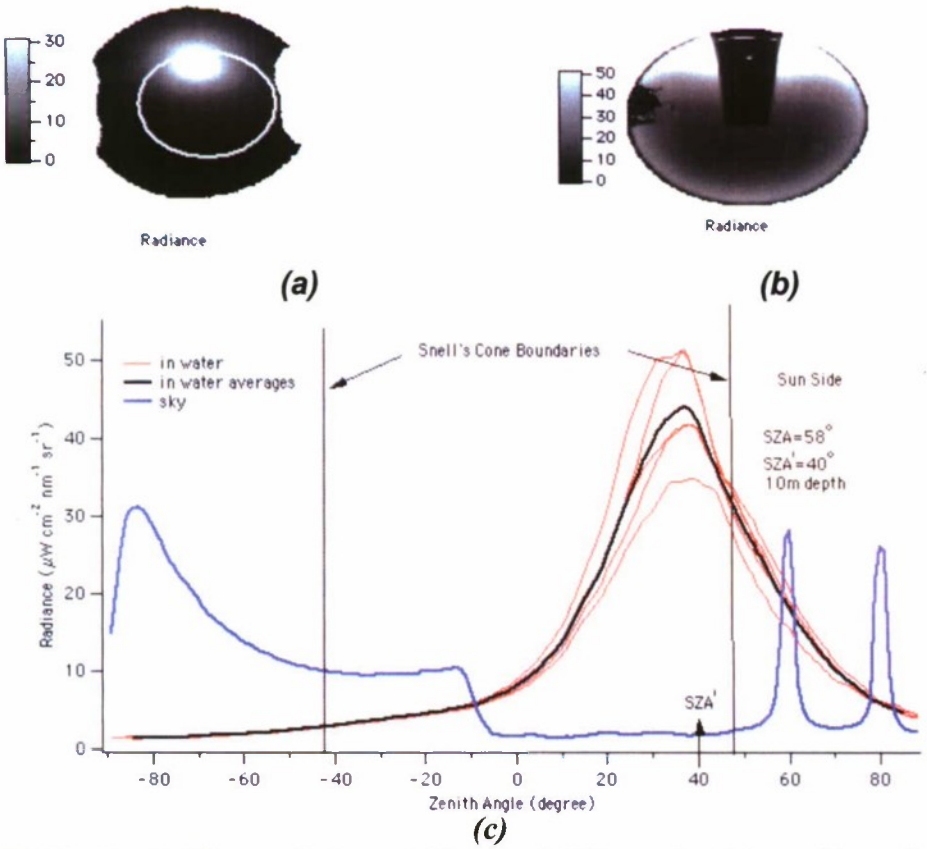

Figure 17. Similar to Figure 11, but at 10m depth. The peak of the radiance has shifted towards the center from the refracted solar zenith direction This effect has commonly been noted in radiance data (Tyler, 1960), and is caused by increased attenuation at larger view zenith angles.

CONCLUSION:

In this paper, we have presented data from the Santa Barbara Channel experiment. From the data and results we have found that the polarization behavior near the surface is mainly dominated by the refracted sky light which strongly depends on the wave-induced curvatures of the water surface. Therefore, near the surface the most of the polarization behavior is seen inside the Snell's cone. At about one meter depth the maximum DOP was found to be about 65% similar to the skylight. As one progresses in the water column the polarization due to light scattering by the water increases, thereby reducing the effect of refracted sky light. Thus, with the increase of the water depth, the polarization behavior outside the Snell's cone increases and the peak of the radiance shifts towards the center (zenith) away from the refracted solar position. However, the maximum DOP decreases with depth. Our data showed that even at 30 meter depths the maximum DOP is about 28%, although it is about 27% less than that of the corresponding sky.

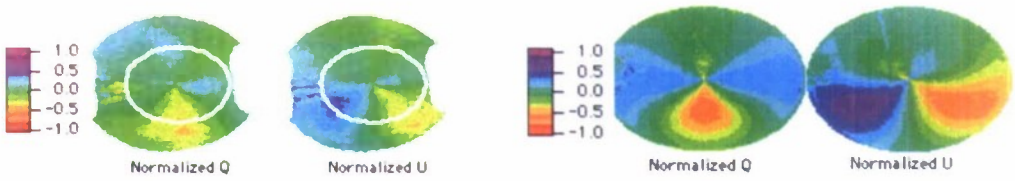

(a) *(b)*

Figure 18. Similar to Figure 12 but at 10 m. More effect of polarization behavior outside the Snell's cone than in 5m depth.

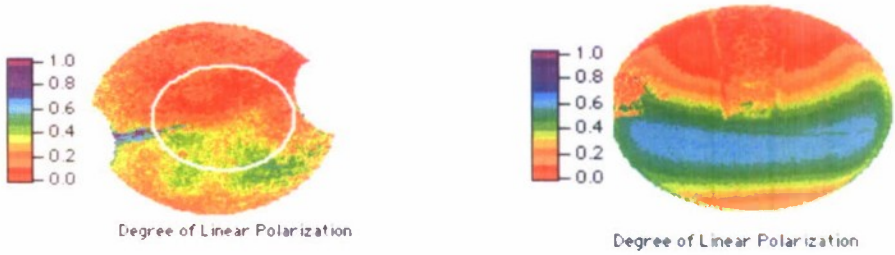

(a) *(b)*

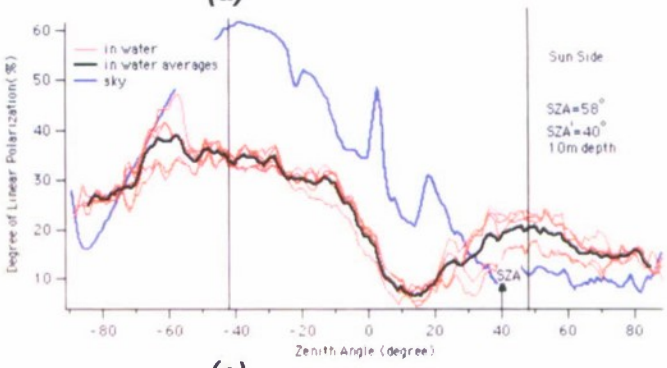

(c)

Figure 19. Similar to Figure 13, but at 10 m. The maximum DOP in water is about 35% and that in air is about 60%.

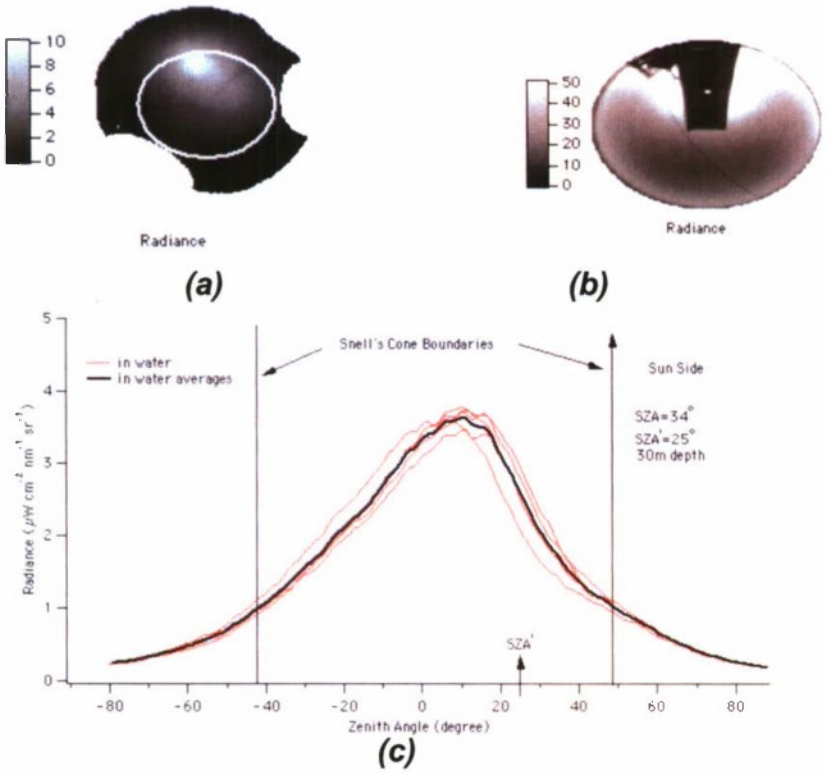

Figure 20. Similar to Fig. 11, but at 30 m. The peak of the radiance has moved even farther towards the center away from the Snell's boundaries and the refracted solar zenith angle.

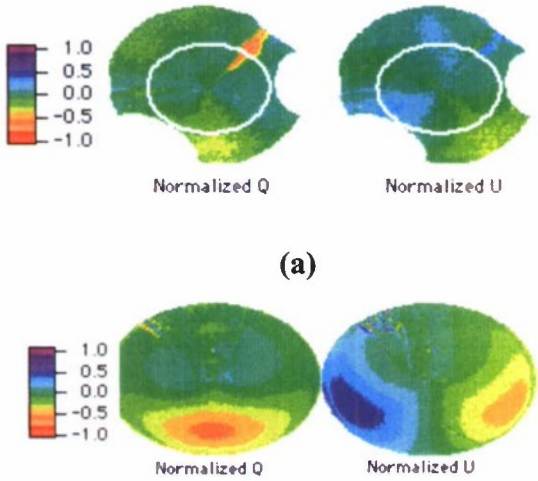

Figure 21. Similar to Fig. 12, but at 30 m. Strong presence of polarization behavior is noticed outside the Snell's cone.

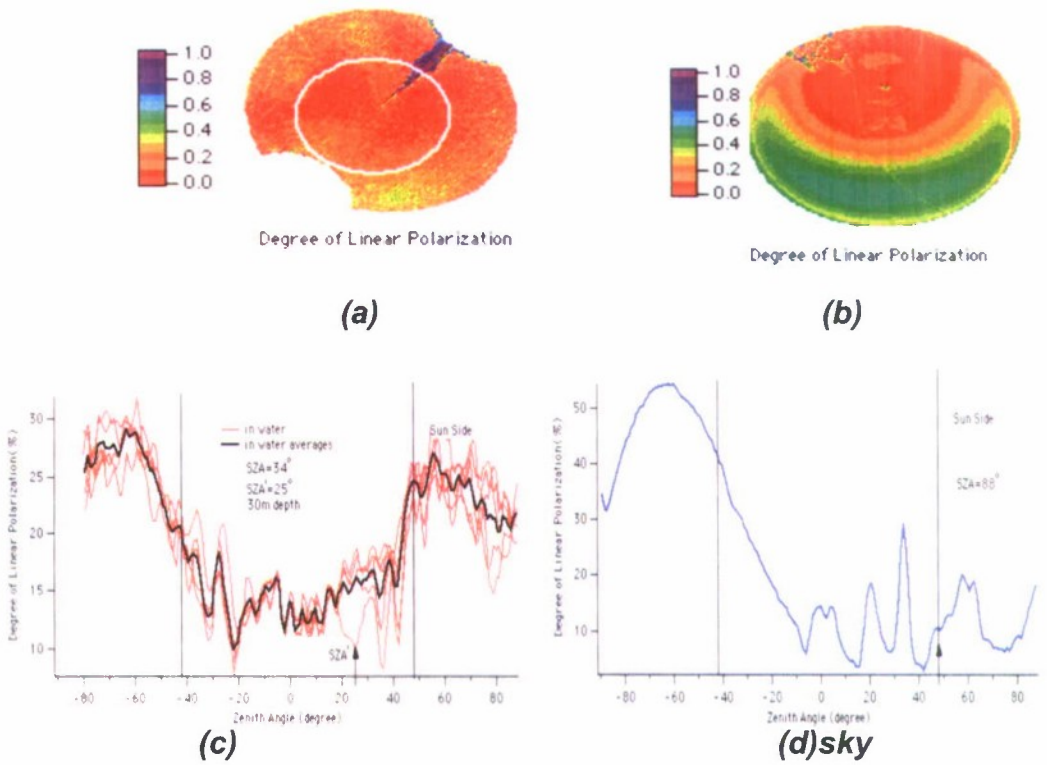

Figure 22. Similar to Fig. 13, but at 30m. The maximum polarization can be seen outside the Snell's cone due to the scattering of light within the water. The maximum DOP in water is about 28% while it is about 55% in air.

REFERENCES:

K.L. Coulson, "Polarization and Intensity of light in the atmosphere", 1988, A. Deepak Publishing, Hampton, Virginia.

H.C. van de Hulst, "Light Scattering by Small Particles", 1981, Dover, New York.

A. Ivanoff, "Polarization measurements in the sea", 1974, in Optical Aspects of Oceanography, N. G. Jerlov and E. Steemann Nielsen, Academic Press, ed. p. 151-175.

A. Ivanoff and T. H. Waterman, "Elliptical polarization of submarine illumination", 1958, J. Mar. Res., **16**., p. 255-282.

Y. Liu, "Measurement of the intensity and polarization of light in the atmosphere", 1996, Ph.D. dissertation, University of Miami, FL.

R. L. Snyder and J. Dera, "Wave-induced light-field fluctuations in the sea", 1970, J. Opt. Soc. Am. 60, 1072-1079.

J. E. Tyler, "Radiance Distribution as a Function of Depth in an Underwater Environment", 1960, Scripps Inst. Oceanogr. Bull. 7: 369-386.

J. S. Tyo, "Optimum linear combination strategy for an N-channel polarization sensitive imaging or vision system", 1998, J. Opt. Soc. Am. A, 15, 359-366.

K. J. Voss and A. L. Chapin, "Upwelling radiance distribution camera system, NURADS", 2005, Optics Express, **13**: 4250 – 4262.

K. J. Voss and Y. Liu, "Polarized radiance distribution measurements of skylight: I. system description and characterization", 1997, Applied Optics, **36** :6083-6094.

K. J. Voss and G. Zibordi, "Radiometric and geometric calibration of a spectral electro-optic "fisheye' camera radiance distribution system", 1989, J. Atmosph. and Ocean. Techn., **6**: 652-662.

T. H. Waterman, "Polarization Patterns in submarine illumination", 1954, Science, 120, p. 927-932.

T. H. Waterman, "Polarization of scattered sunlight in deep water", 1955, Deep-Sea Res., p. 426-434.

Papers resulting from this grant:

K. J. Voss and N. Souaidia, "POLRADS: polarization radiance distribution measurement system", Optics Express, **18**, 19672-19680 (2010). [REFEREED]

H. Zhang and K. J. Voss, "Bi-directional reflectance and polarization measurements on packed surfaces of benthic sediments and spherical particles", Optics Express, 2009, **17**:5217-5231 (doi:10.1364/OE.17.005217). [REFEREED]

H. Zhang and K. J. Voss, "Bi-directional reflectance measurements of closely packed natural and prepared particulate surfaces" in *Light Scattering Reviews*, Vol. 3, pgs. 279-327, 2008. [BOOK CHAPTER]

Presentations resulting from this grant:

K. J. Voss and N. Souaidia, "A new tool to measure the upwelling polarized spectral radiance distribution", AGU Ocean Science meeting, Orlando, Fl. March 2008. **POSTER**

Voss, K. J., P. Bhandari, L. Logan, "A new spectral polarized radiance distribution camera system, DPOL", Ocean Optics X1X, Barca, Italy, October 2008. **POSTER**

K. J. Voss, P. Bhandari, L. Logan, "Polarized radiance distribution in the near surface region", 2010 Ocean Sciences Meeting, Portland, Or., February 2010. **TALK**

M. L. Banner, C. J. Zappa, J. Gemmrich, P. Bhandari, K. J. Voss, M. Lewis, "Breaking Waves and their Influence on Subsurface Light Fluctuations", 2010 Ocean Sciences Meeting, Portland, Or., February 2010. **POSTER**

K. J. Voss, "Polarized radiance distribution in the near surface region", ONR Ocean Optics Program Review, Portland, Or., February 2010. **TALK**

P. Bhandari, K. J. Voss, L. Logan, "The variation of the polarized downwelling radiance distribution with depth in coastal water", Ocean Optics XX, Anchorage, Ak., October 2010, **TALK (given by Bhandari) and POSTER.**

K. Voss, A. Gleason, H. Gordon, G. Kattawar, Y. You, "The discovery of non-principal-plane neutral points in the in-water upwelling polarized light field", Ocean Optics XX, Anchorage, Ak, October 2010. **TALK and POSTER**

R. Van Dommelen, J. Wei, M. Lewis, K. Voss, "Instrumentation, characterization and validation of a high dynamic range radiance camera", Ocean Optics XX, Anchorage, Ak., October 2010. **POSTER**

G. Zibordi and K. J. Voss, "Field Radiometry and Ocean Color Remote Sensing",

Oceans From Space 2010, Venice, Italy, April, 2010. **Invited Talk (given by Zibordi)**

Papers in progress (submitted):

K. J. Voss, A. C. Gleason, H. R. Gordon, G. Kattawar, Y. You, "Discovery of non-principal plane neutral points in the in-water upwelling polarized light field", Submitted to Optics Express, Nov 2010.

T. D. Dickey, G. W. Kattawar, and K. J. Voss, "Shedding new light on light in the ocean", Submitted to Physics Today, Dec 2010.

H. Zhang and K. J. Voss, "On Hapke photometric model predictions on reflectance of closely packed particulate surfafces", Submitted to Icarus, Dec 2010.